



Universiteit
Leiden
The Netherlands

Preparing for CADASIL therapy

Gravesteijn, G.

Citation

Gravesteijn, G. (2020, October 28). *Preparing for CADASIL therapy*. Retrieved from <https://hdl.handle.net/1887/137984>

Version: Publisher's Version

License: [Licence agreement concerning inclusion of doctoral thesis in the Institutional Repository of the University of Leiden](#)

Downloaded from: <https://hdl.handle.net/1887/137984>

Note: To cite this publication please use the final published version (if applicable).

Cover Page



Universiteit Leiden



The handle <http://hdl.handle.net/1887/137984> holds various files of this Leiden University dissertation.

Author: Gravesteijn, G.

Title: Preparing for CADASIL therapy

Issue Date: 2020-10-28

Chapter 2

Progression and classification of granular osmiophilic material (GOM) deposits in functionally characterized human *NOTCH3* transgenic mice

Gido Gravesteijn
Leon P. Munting
Maurice Overzier
Aat A. Mulder
Ingrid Hegeman
Marc Derieppe
Abraham J. Koster
Sjoerd G. van Duinen
Onno C. Meijer
Annemieke Aartsma-Rus
Louise van der Weerd
Carolina R. Jost
Arn M.J.M. van den Maagdenberg
Julie W. Rutten*
Saskia A.J. Lesnik Oberstein*

ABSTRACT

CADASIL is a *NOTCH3*-associated cerebral small vessel disease. A pathological ultrastructural disease hallmark is the presence of *NOTCH3*-protein containing deposits called granular osmiophilic material (GOM), in small arteries. How these GOM deposits develop over time and what their role is in disease progression is largely unknown. Here, we studied the progression of GOM deposits in humanized transgenic *NOTCH3*^{Arg182Cys} mice, compared them to GOM deposits in patient material, and determined whether GOM deposits in mice are associated with a functional CADASIL phenotype. We found that GOM deposits are not static, but rather progress in ageing mice, both in terms of size and aspect. We devised a GOM classification system, reflecting size, morphology and electron density. Six-month-old mice showed mostly early stage GOM, whereas older mice and patient vessels showed predominantly advanced stage GOM, but also early stage GOM. Mutant mice did not develop the most severe GOM stage seen in patient material. This absence of end-stage GOM in mice was associated with an overall lack of histological vascular pathology, which may explain why the mice did not reveal functional deficits in cerebral blood flow, cognition and motor function. Taken together, our data indicate that GOM progress over time, and that new GOM deposits are continuously being formed. The GOM staging system we introduce here allows for uniform GOM deposit classification in future mouse and human studies, which may lead to more insight into a potential association between GOM stage and CADASIL disease severity, and the role of GOM in disease progression.

INTRODUCTION

Deposition of granular osmiophilic material (GOM) is the vascular pathological hallmark of CADASIL, which is the most prevalent hereditary small vessel disease¹ and is caused by missense mutations in the *NOTCH3* gene.^{2,3} GOM have been shown to contain NOTCH3 ectodomain (NOTCH3^{ECD}) and extracellular matrix proteins,^{4–6} and can be visualized ultrastructurally in the tunica media of small arteries and capillaries. These electron dense GOM deposits are located in the basement membrane of mural cells, i.e. vascular smooth muscle cells and pericytes.^{7–11} In both manifest and pre-manifest CADASIL patients, GOM deposits are present not only in brain vessels, but also in vessels of other organs, such as the skin.^{11–13} Other CADASIL-associated vascular pathology includes mural cell degeneration, smooth muscle actin (SMA)-positive (neo)intima formation, fibrosis, and vessel wall thickening.^{14–19} These vascular alterations are associated with compromised cerebrovascular reactivity (CVR)^{20,21} and reduced cerebral blood flow (CBF), and eventually lead to mid-adult onset of recurrent strokes, vascular cognitive impairment and ultimately dementia.¹ Brain MRI reveals progressive symmetrical white matter hyperintensities, lacunes, microbleeds and brain atrophy.¹

We have previously described that our humanized CADASIL transgenic *NOTCH3*^{Arg182Cys} mouse model, which overexpresses human mutant NOTCH3 protein from a genomic construct, shows granular NOTCH3^{ECD} immunostaining as early as 4 weeks of age, while GOM deposits first appear around 6 months of age.²² However, little is known about how GOM deposits evolve over time and what their relation is to other CADASIL-associated vascular pathology and vascular dysfunction. Here, we performed a longitudinal study of GOM pathology in the transgenic *NOTCH3*^{Arg182Cys} mice. In addition, we assessed cerebrovascular, motor and cognitive function in these mice.

METHODS

Mice

Transgenic mice were used that harbour the human full length *NOTCH3* gene (located on a 143 kb BAC construct) in either the wildtype or the mutant (c.544C>T, p.Arg182Cys) form, generated on a C57BL/6J background.²² Mice were bred at the animal facility of the Leiden University Medical Center and housed individually under standard conditions, i.e. a 12-hour light/dark cycle with food and water available *ad libitum*.

Three different mouse strains were used, with various human *NOTCH3* expression levels: 100% for wildtype mice (tgN3^{WT100}), and 100% and 350% for mutant mice (tgN3^{MUT100} and tgN3^{MUT350}, respectively).²² Non-transgenic littermates were used as additional controls. A prospective study with 6-8 mice per group was performed to study body weight and motor function at various time points (1.5, 3, 6, 12, 16 and 20 months) and cerebral hemodynamics, cognition and immunohistochemical staining was studied at 20 months. Three mice had to be sacrificed before the end of the study; one due to an eye infection (tgN3^{WT100}, at 15 months), one due to having a wound on its back (tgN3^{MUT350}, at 19 months), and one due to low body weight (tgN3^{MUT100}, at 20 months). In addition to the prospective study, tgN3^{MUT350} mice were sacrificed at the age of 1.5 (n=1), 3 (n=1), 6 (n=2), 12 (n=2) and 20 (n=2) months for electron microscopy (EM) studies.

Electron microscopy

In addition to mouse brain, post-mortem brain tissue was obtained from three CADASIL patients (deceased at age 59, 66, and 69 years) for comparison with human pathology. Mouse (frontal lobe grey matter) and human (frontal lobe grey matter) brain tissue was fixed overnight at 4°C in 1.5% glutaraldehyde and 1% paraformaldehyde (pH=7.4). Tissue blocks of ≤ 1 mm³ were post-fixed for 90 minutes in 2% osmium tetroxide and 2% potassium ferrocyanide after filtrating the post-fixative through a 0.2- μ m filter. After post-fixation, the tissue was washed for 30 minutes in MilliQ and dehydrated in a series of ethanol (70%, 80% and 90%) for 30 minutes each and twice for 1 hour in 100% ethanol. Blocks were incubated for 10 minutes in propylene oxide, 2 hours in propylene oxide and Epon LX-112 (1:1) and finally for 2 hours in propylene oxide and Epon LX-112 (1:2). Subsequently, the epon was polymerized for 48 hours at 70°C.

One- μ m thick sections were checked for the presence of blood vessels by light microscopy. Then, areas with high blood vessel density were selected for further analysis with EM, i.e. 80-nm sections were collected on a one hole grid and subsequently stained with uranyl acetate and lead citrate. Images were acquired with a digital camera (One View, Gatan Inc., Pleasanton, CA) mounted on a 120 kV transmission electron microscope (Tecnai T12 with a twin objective lens, Fei Inc, Hillsborough, OR). Overviews of relatively large regions on the specimen that contained abundant numbers of cross-sections of vessels were collected by stitching many individual images together (40,000-60,000 nm²) using software described earlier.²³ Stitched images were examined using Aperio ImageScope (version 10.0.35).

GOM analysis

The number of GOM deposits was counted per vessel and expressed as counts per 100 μ m vessel circumference. Vessel circumference was approximated using the formula of oval circumference (Ramanujan's approximation for ellipse circumference = $\pi[3(a+b)$

- $\sqrt{((3a+b)*(a+3b))}$ where a and b were defined as the major diameter (a) and minor diameter (b) for each vessel between endothelial basement membranes. GOM deposits were studied in vessels with a minor diameter < 8 μm , referred to as microvessels, as these were the most abundant in the stitched images. Twenty-three to 84 microvessels were studied per time point (1.5, 3, 6, 12 and 20 months). Width of the basement membrane was determined averaging 40 measurements in two ntg mice and two tgN3^{MUT}350 mice each. In the human brain sample, 21 microvessels were analysed. Also, the GOM deposit area was measured using ImageJ after manually drawn region-of-interests around GOM deposits.

Immunohistochemistry

Two 5- μm coronal frontal brain sections per mouse (approximately at the height of the infundibulum) and human brain sections of frontal white matter were analysed with immunohistochemistry. NOTCH3^{ECD} staining was performed as described before.²² Smooth muscle actin (SMA) staining was performed after pre-treatment with trypsin for 30 minutes at 37°C and washed three times for 5 min with PBS. The primary antibody (Alpha-Smooth Muscle Actin, 1:4000, goat polyclonal, NB300-978, Novus Biologicals) was incubated overnight at room temperature. The secondary antibody (Rabbit Anti-Goat IgG, biotinylated, 1:400, Jackson Immunoresearch Lab. Inc.) was incubated for 1 hour at room temperature and developed with the Vectastain Elite ABC HRP Kit (PK-6100, Vectorlabs) for 30 min at room temperature. Finally, slices were stained with 0.05% 3,3'-diaminobenzidine (DAB, Sigma) supplemented with 0.0045% H₂O₂ for 10 min and stained with Harris' hematoxylin solution (diluted 1:3, Merck) for 5 seconds. Sections were Verhoeff-Van Gieson and Periodic Schiff Acid stained using the Artisan Link Pro staining machine (DAKO, Agilent), and Van Gieson stained as described previously.²⁴ Sections were stained with Klüver-Barrera luxol fast blue to quantify white matter vacuolization (Supplementary Methods 4).

Microscopy imaging was performed with the Keyence BZ-X710 (Keyence). Using 20 times magnification, full colour images were taken of the complete section at 1-ms capture time. Images were stitched by Keyence BZ-X Analyzer software version 1.3.0.3 to obtain one high resolution full brain image per section. The SMA positive area was determined using a Colour Threshold (Hue 0-50; Saturation 0-255; Brightness 0-175) in ImageJ, and expressed as percentage of total brain surface of the section.

Neuroimaging, cerebrovascular reactivity, cognition and motor function

At the age of 20 months, neuroimaging (T2W, FLAIR, SWI, cerebral hemodynamics) was performed under medetomidine anaesthesia using a 7 Tesla MRI (Bruker PharmaScan), see also Supplementary Methods 1. In short, absolute cerebral blood flow (CBF) was measured using arterial spin labeling (ASL)-MRI during a 7-minute baseline and a 7-minute CO₂ challenge, using the measured signal difference between the labelled and control

images in three brain slices. Absolute CBF at baseline and absolute CBF at challenge were quantified during the last 140 seconds of baseline and challenge, respectively. Absolute CBF increase was calculated as well as the cerebrovascular reactivity (CVR), which was defined as the relative cerebral blood flow (CBF) increase. One non-transgenic mouse was excluded from neuroimaging analysis due to a poor hemodynamic response to anaesthesia.

A Morris Water Maze protocol was used to assess cognitive function in 20-month-old mice, starting 2 weeks before neuroimaging assessment (Supplementary Methods 2.2). In short, during the training phase, mice were trained to find a hidden platform in the north-west quadrant of a circular swimming pool, while at the reversal training phase, mice were retrained to find a hidden platform in the south-east quadrant. Path length of the mice was determined between release in the pool and finding the hidden platform. Motor function was determined by analysing speed on a rotarod, on a beam and during swimming in the Morris water maze (Supplementary Methods 2.3). Motor and cognitive mouse experiments were performed by the same experienced researcher.

Statistical analyses

Differences between groups were analysed using one-way ANOVA analyses with Tukey's post-hoc correction. The increase in GOM area over time, as well as the association between baseline CBF and CVR were analysed using simple linear regression. All statistical analyses were two-sided tests with threshold for statistical significance of 0.05, using the IBM SPSS Statistics version 23.0.0.2 software.

RESULTS

Temporal GOM assessment

GOM appearance, size and count were studied in brain microvessels of tgN3^{MUT}350 mice at the age of 1.5, 3, 6, 12, and 20 months. GOM deposits were first observed at the age of 6 months, appearing as small, round deposits in the basement membrane of mural cells, which were sometimes only slightly more electron dense than the surrounding basement membrane (Figure 2.1a). At 12 months, most GOM deposits were larger and more electron dense. At 20 months, large amorphous GOM deposits were observed, which spanned the full width of the basement membrane (Figure 2.1b). Irrespective of age, GOM deposits were predominantly (85%) located on the abluminal side of mural cells, bulging out the basement membrane and thereby leaving an indentation in the adjacent mural cell. Between 6 and 20 months, GOM size increased ($b=0.0030 \mu\text{m}^2/\text{month}$, $P=0.002$) (Figure 2.1c), GOM count more than doubled (0.9 to 2.4 GOM/100 μm) and the percentage of GOM-positive vessels increased from 26% to 39%.

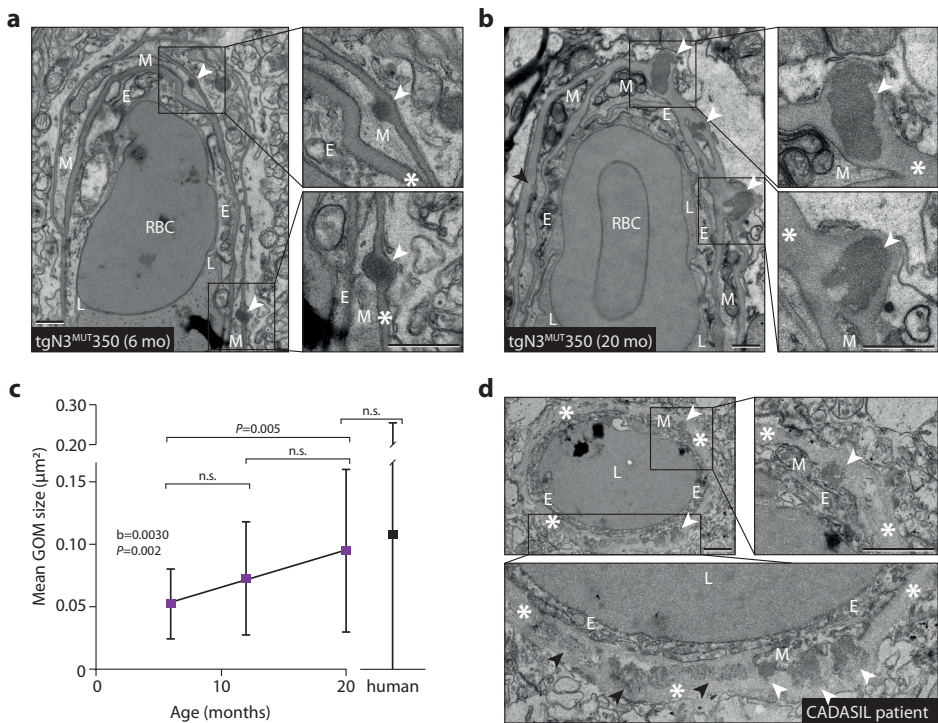
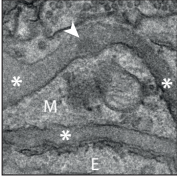
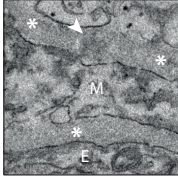
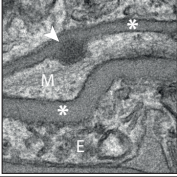
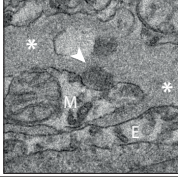
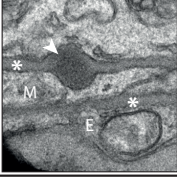
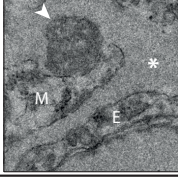
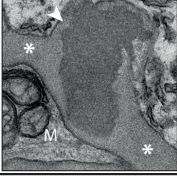
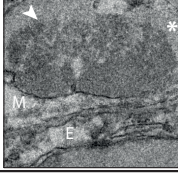
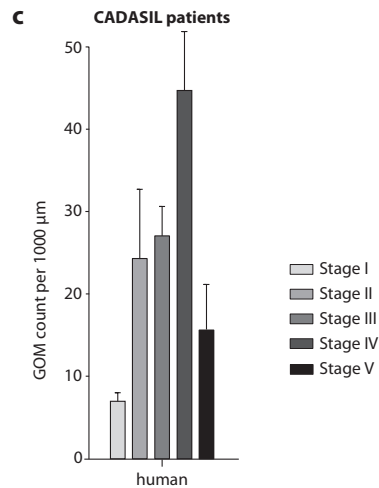
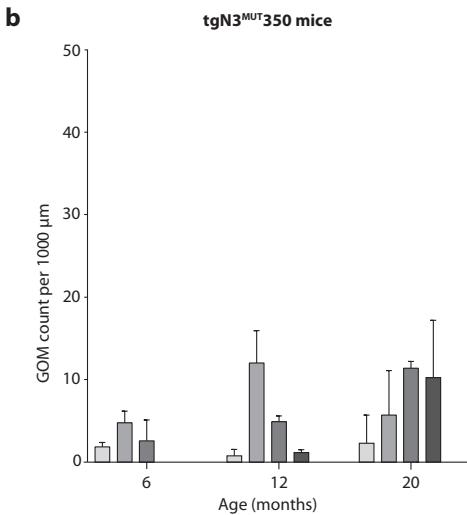


Figure 2.1: Progression of GOM in brain vessels of CADASIL mice

(A) Electron microscopy (EM) of brain vessels of tgN3^{MUT350} mice at the age of 6 months reveals round, electron dense GOM deposits near mural cells (white arrowheads). (B) EM at the age of 20 months shows larger and amorphous GOM deposits (white arrowheads), but also a small GOM deposit (grey arrowhead). The basement membrane bulges out at the location of a GOM deposit, but is otherwise not thickened in vessels of tgN3^{MUT350} mice. Mural cells have a normal aspect, i.e. without electron lucent vacuoles, large intracellular vesicles or a shrunken appearance. (C) Analysis of the size of GOM deposits in mouse brain vessels shows a significant increase in GOM size between the age of 6 and 20 months ($b=0.0030 \mu\text{m}^2/\text{month}$, $P=0.002$). Average GOM size in brain vessels of deceased CADASIL patients ($0.108 \pm 0.148 \mu\text{m}^2$, $n=292$ GOM deposits) was higher than in mice ($0.095 \pm 0.065 \mu\text{m}^2$, $n=31$ GOM deposits), but this difference was not statistically significant ($P=0.634$) due to the large variability in GOM size in human brain vessels. (D) Post-mortem analysis of CADASIL brain microvessels ($n=3$ patients) showed extensive GOM pathology, with deposits in all vessels, both bulging into adjacent mural cells (white arrowheads) and located centrally in the thickened basement membrane further away from mural cells (grey arrowheads). In contrast to mice, GOM deposits in the CADASIL patient had a more granular aspect with heterogeneous electron density. CADASIL patient brain vessels had a thickened basement membrane and mural cells showed signs of degeneration, such as a shrunken appearance. Arrowhead = GOM; Asterisk = basement membrane; E = Endothelial cell; M = Mural cell; n.s. = non significant; RBC = Red blood cell. Bar represents $1 \mu\text{m}$. Graph represents mean \pm SD.

Based on these observations, we categorized GOM deposits into various stages that reflect relative size, morphology, electron density and the GOM deposit-induced bulging of the basement membrane with concomitant indentation of adjacent mural cells (Figure 2.2a).

Stage	tgN3 ^{MUT350} mouse	CADASIL patient	Description
I			<ul style="list-style-type: none"> - GOM deposits are <i>smaller</i> than normal width of BM - GOM deposits are round or elliptical - Minimal bulging of BM and minimal indentation of mural cell near GOM - GOM deposits are <i>only slightly more electron-dense</i> than surrounding extracellular matrix
II			<ul style="list-style-type: none"> - GOM deposits are <i>smaller</i> than normal width of BM - GOM deposits are round or elliptical - Bulging of BM with indentation of mural cell near GOM - GOM deposits are electron-dense
III			<ul style="list-style-type: none"> - GOM deposits are <i>larger</i> than normal width of BM - GOM deposits are round or elliptical - Bulging of BM, and/or overall thickened BM (in human) - Larger indentation of mural cell near GOM - GOM deposits are electron-dense
IV			<ul style="list-style-type: none"> - GOM deposits are <i>larger</i> than normal width of BM - GOM deposits are <i>amorphous</i> or have <i>bizarre shapes</i> - Bulging of BM, and/or overall thickened BM (in human) - Larger indentation of mural cell near GOM - GOM deposits are electron-dense
V	not observed in mice		<ul style="list-style-type: none"> - Two or more stage IV GOM deposits confluence into a patch of <i>confluent GOM</i> - Bulging of BM, and/or overall thickened BM (in human) - Mural cells can have two or more subtle indentations, reflecting two or more GOM deposits



◀ Figure 2.2: A 5-stage GOM classification system for CADASIL

(A) Classification system for GOM deposits based on size, morphology and electron density. Per stage, examples are shown from brain vessels of $\text{tgN3}^{\text{MUT}350}$ mice and of deceased CADASIL patient. In each example, the bottom of the image points towards the luminal side of the vessel. Cells were denoted as endothelial cells (E) or mural cells (M) based on interpretation of the morphology of cells as a whole within the vessel. (B) Staging of GOM deposits in brain vessels of $\text{tgN3}^{\text{MUT}350}$ mice. At 6 months of age, stages I-III GOM deposits were present, while at 20 months mainly stages III-IV GOM deposits were observed. (C) Staging of GOM in brain vessels from deceased CADASIL patients. GOM deposits of all stages were observed, but stage IV GOM deposits were most abundant. Overall GOM count in patients was higher than in mice. Arrowhead = GOM; Asterisk = basement membrane; E = Endothelial cell; M = Mural cell.

Stage I GOM deposits are small and slightly electron dense and induce minimal mural cell indentation. Stage II and III GOM deposits are more electron dense, induce basement membrane bulging with mural cell indentation, and are within (II) or extend beyond (III) the normal width of the basement membrane (~150 nm). Stage IV GOM deposits extend beyond the normal width of the basement membrane and are amorphous. At 6 months of age, stage I-III GOM deposits were observed in $\text{tgN3}^{\text{MUT}350}$ mice. At 12 months, the first stage IV GOM appeared. At 20 months, the majority of the GOM were at stages III and IV (Figure 2.2b), but stage I GOM deposits were also observed. This suggests that new GOM deposits are continuously being formed, and that once formed, the initially small round GOM deposits progress over time into large amorphous deposits.

Next, we compared GOM in brain tissue of three CADASIL patients to GOM in 20-month-old $\text{tgN3}^{\text{MUT}350}$ mice (Figure 2.1d). Almost all (96%) of the analysed microvessels in the patients contained GOM deposits, whereas GOM deposits were observed in only 39% of microvessels in the mutant mice. In human brain material, like in mice, GOM deposits of all stages were observed, but stage IV GOM deposits were most frequent (Figure 2.2c). In addition, the patients' microvessels contained large confluent patches of GOM (stage V GOM) that were not observed in the mice. Of note, the electron density of GOM deposits in the patients' microvessels was less homogeneous than of GOM in mice. GOM deposits in patient microvessels either bulged out of the basement membrane and thereby left an indentation in the adjacent mural cell, or were located further away from any recognisable mural cells within an overall thickened basement membrane. In contrast, GOM deposits in mice were always located close to the mural cell, often in indentations of the mural cell formed by the GOM deposits.

Other CADASIL-associated vessel wall and brain parenchyma changes

Despite large GOM deposits and extensive granular $\text{NOTCH3}^{\text{ECD}}$ staining at 20 months (Figure 2.3a), $\text{tgN3}^{\text{MUT}350}$ mice did not show basement membrane thickening ($\text{tgN3}^{\text{MUT}350}$ $0.145 \pm 0.050 \mu\text{m}$, ntg $0.148 \pm 0.055 \mu\text{m}$, $P=0.73$) and there were no signs of mural

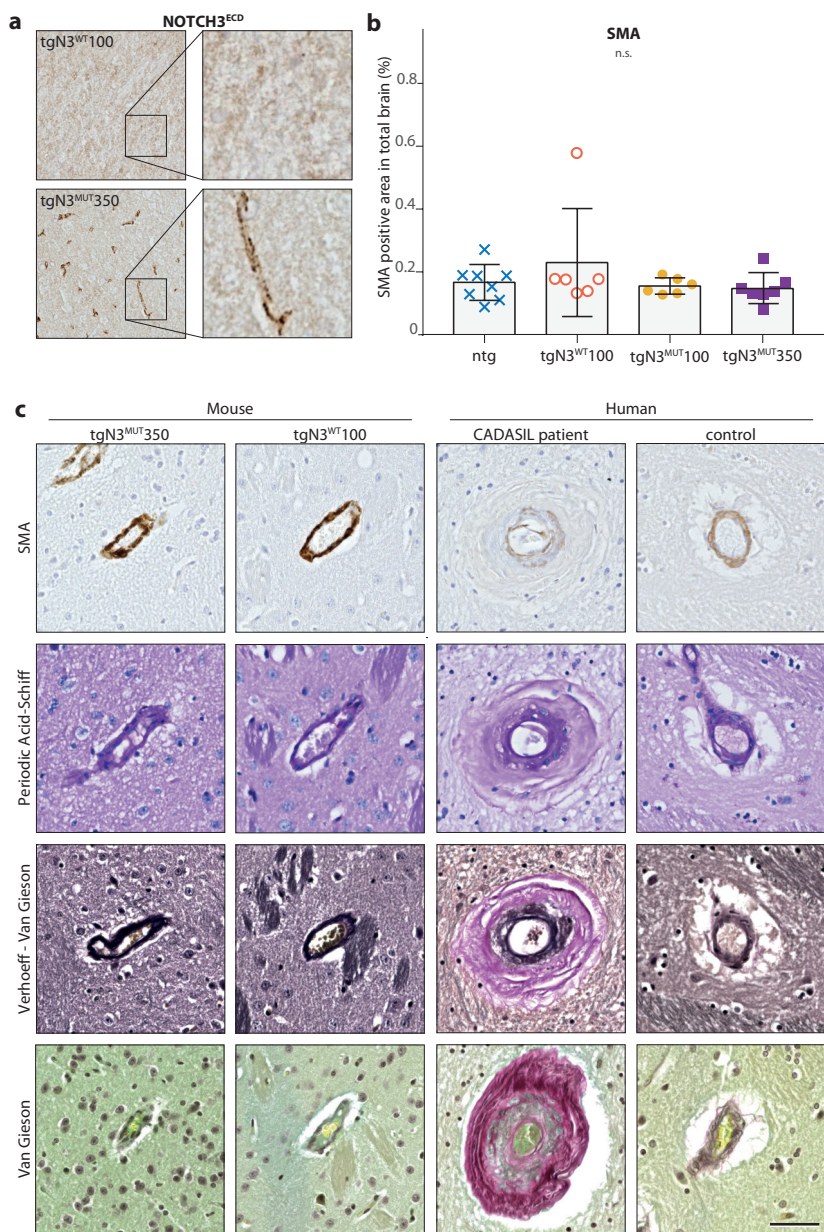


Figure 2.3: No vessel wall thickening or reduced SMA staining in mice expressing mutant human NOTCH3 protein
 (A) Mutant mice (tgN3^{MUT350}) show granular NOTCH3^{ECD} deposits in brain vessels, which were not observed in wildtype mice (tgN3^{WT100}). (B) SMA content in brain was similar in the four mouse strains. One tgN3^{WT100} brain section contained a large artery which was longitudinally cleaved, resulting in a high SMA positive area. (C) The pattern of SMA immunoreactivity in the vessel wall was similar between the four groups (only images of the tgN3^{MUT350} and tgN3^{WT100} strains are shown), while the white matter of CADASIL patients ▶

degeneration, such as electron lucent vacuoles, large intracellular vesicles or a shrunken appearance (Figure 2.1a,b). Also, there was no difference in the amount or pattern of SMA staining between mutant and wildtype mice (Figure 2.3b,c). In addition, Van Gieson's, Verhoeff-Van Gieson's, and Periodic Acid-Schiff staining did not show vessel wall thickening, in contrast to our observations in vessels of the CADASIL patients (Figure 2.3c). There was no difference in white matter vacuolization between wildtype and mutant mice (Supplementary Data 2.2).

Cerebral blood flow, cerebrovascular reactivity and neuroimaging

Next, we assessed cerebral blood flow (CBF) dynamics in 20-month-old mice using ASL-MRI with CO₂ as vasodilative stimulus (Figure 2.4a). Compared to non-transgenic and wildtype mice, mutant mice (tgN3^{MUT}100 and tgN3^{MUT}350) did not show a significant difference in CVR, which was defined as relative CBF increase upon challenge (Figure 2.4b,d), absolute CBF increase upon challenge (Figure 2.4c,e), or in CBF at baseline (Figure 2.4f). There was, however, a non-significant trend towards a reduced CVR and a slightly increased baseline CBF in the tgN3^{MUT}350 mice. Differences in baseline CBF likely contributed to the observed differences in CVR, as there was an inverse correlation between baseline CBF and CVR ($s=-0.69$, $P<0.001$, Supplementary data 2.1). Separate analysis of CBF and CVR for cortex and subcortex showed similar results (Supplementary data 2.3 and 2.4). High-resolution T2w, FLAIR and SWI MRI scans of mouse brains did not show white matter hyperintensities, lacunes, or microbleeds. Also, gadolinium enhancement showed the typical pattern of contrast enhancement in and around the ventricles, but no differences were observed between tgN3^{MUT}350 and wildtype mice (Supplementary data 2.5).

Cognition and motor function

Motor function, as assessed by rotarod running, beam walk and swimming speed, did not differ between mutant and wildtype mice at any of the time points (Supplementary data 2.6). In the Morris water maze tests, mutant mice did not show signs of impaired memory formation. If anything, tgN3^{MUT}350 mice performed slightly better at some of the tasks (Figure 2.5).

► showed less and fragmented SMA immunoreactivity, with SMA-positive areas in the intima. PAS, VvG and VG staining showed similar brain vessel staining patterns between the four groups, but the brain vessels of the CADASIL patients showed a clearly thickened vessel wall, with a positive PAS staining (carbohydrates), VvG staining (collagenous material red; elastic material black) and VG staining (collagenous material red). SMA = smooth muscle actin; n.s. = non significant; PAS = Periodic Acid-Schiff staining; VG = Van Gieson's staining; VVG = Verhoeff-Van Gieson's staining. Bar represents 50 μ m. Graph represents mean \pm SD.

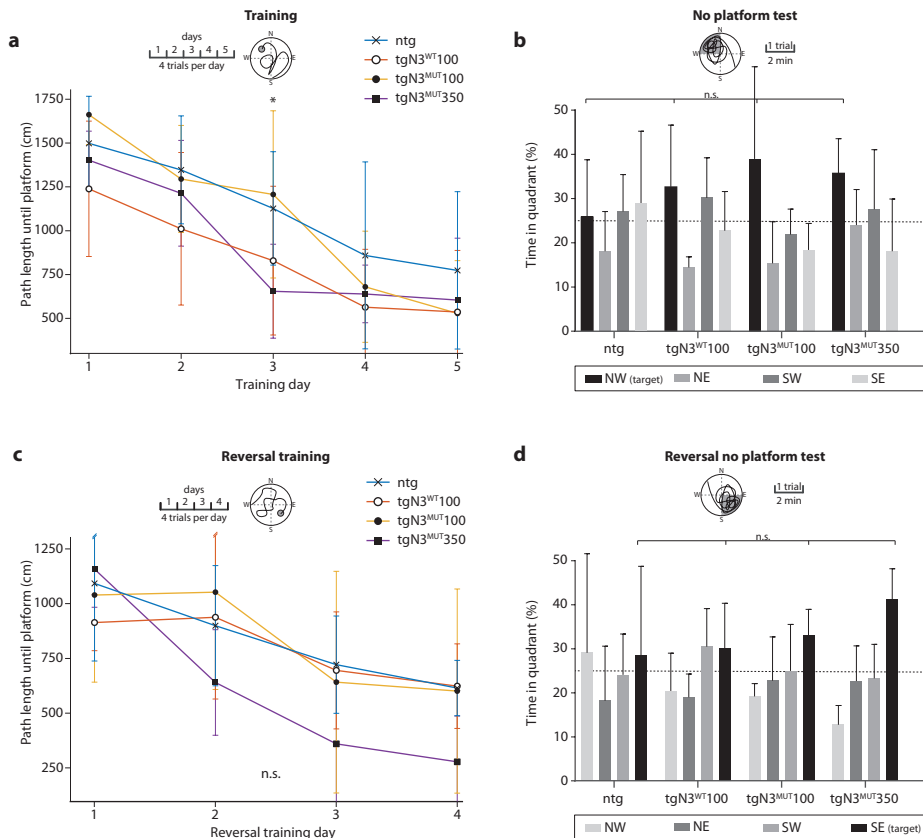


Figure 2.5: CADASIL mice do not show cognitive dysfunction

(A) The path length until finding a hidden platform in the water maze was similar for all strains (ntg, tgN3^{WT100}, tgN3^{MUT100}, tgN3^{MUT350}). (B) After the 5 training days, mice underwent one trial without a platform. The time spent in the target quadrant (NW) was similar between the groups ($P=0.46$; ANOVA). (C) A 4-day reversal training phase with the platform hidden in the south-east quadrant showed no significant differences in path length until finding the hidden platform between the groups ($P=0.14$ on day 4; ANOVA). (D) Time in target quadrant after the reversal training was similar between the groups ($P=0.09$; ANOVA). Graphs represent mean \pm SD; n.s. = non significant; * $P<0.05$.

DISCUSSION

We investigated the development of GOM deposits over time in a transgenic mouse model of CADASIL, which overexpresses mutant human NOTCH3 protein from a large genomic construct. GOM deposits evolved with respect to size, morphology and number in microvessels of the mutant mouse brain. Here, we propose a 5-stage GOM classification system to facilitate uniform analysis and description of GOM deposits and show that this staging can also be used to systematically classify GOM in vessels of CADASIL patient material.

The GOM deposits observed in aged mice (20 months) included stages I-IV, i.e. from small, circumscribed deposits within the basement membrane (stage I), to large, amorphous GOM that induced bulging of the basement membrane (stage IV). As mice aged 6 months only showed stages I-III GOM, individual GOM deposits seem to increase in size and become increasingly amorphous over time, and new GOM seem to be continuously formed. This is further illustrated by the observation that GOM deposits of stage I and II are also present in post-mortem CADASIL patient brain microvessels, next to the more extensive GOM pathology, including patches of confluent GOM (stage V).^{7,25,26}

Although many studies have reported the presence and morphology of GOM in CADASIL patients,^{9,11–13,25,27–30} little is known about how GOM deposits progress over time. Brulin *et al.* analyzed GOM in skin biopsies of CADASIL patients of different ages, and found that the number of GOM deposits increase up to 50 years of age, but also found that the number of GOM seems to decrease in elderly patients.¹¹ The latter may either be attributed to other end-stage vessel wall changes hampering the visualization of GOM, or because GOM seem to become confluent and disintegrate over time.²⁶ Whether different GOM stages in skin biopsies of CADASIL patients are associated with disease severity and disease progression, therefore, remains to be determined. If so, the proposed GOM classification system may aid future efforts to monitor and predict disease progression at the individual patient level.

In our humanized CADASIL mouse model and in a rat Notch3 CADASIL mouse model, GOM deposits are observed several months after the first signs of NOTCH3^{ECD} positive granular immunostaining,^{22,30} suggesting that NOTCH3^{ECD} granules may act as seeds for GOM development. Since NOTCH3^{ECD} aggregates attract extracellular matrix proteins that are components of GOM deposits, such as TIMP3 and clusterin,^{4,5} there seems a direct temporal relation between NOTCH3^{ECD} aggregates and the formation of GOM deposits. Delineating molecular differences between early- and end-stage GOM deposits may help to understand the sequence of events in CADASIL vascular pathology, and perhaps the identification of early therapeutic targets.

Whereas the CADASIL mice in our study seem to faithfully replicate early signs of disease pathology (*NOTCH3*^{ECD} accumulation and GOM deposition), we did not observe other CADASIL-associated disease features which have been observed in other CADASIL mouse models, such as vessel wall thickening, changes in SMA staining, mural cell degeneration and blood brain barrier leakage.^{7,9,14,15,17,31} In line with this, we previously showed that our mutant mice do not show brain parenchyma pathology at age 20 months, which we confirmed in this study using high resolution T2W neuroimaging.²² Furthermore, we extended the characterization of the mice with functional tests, which did not reveal any cognitive or motor dysfunction. Our cerebral blood flow studies showed a small, not significant, reduction in CVR in tgN3^{MUT}350 mice, while studies in other, genetically different, CADASIL mouse models did show a reduced CVR.^{8,30,32} It may be relevant that we used a different method to anaesthetize mice and also to measure CVR, namely an ASL-based MRI approach. Although less sensitive in detecting small CVR changes, the advantage of ASL-MRI is that it allows for absolute perfusion quantification and detection of differences in baseline CBF. In that way, we found that the slight reduction of CVR in tgN3^{MUT}350 mice could at least partially be explained by a higher CBF at baseline. Future research is needed to determine whether the differences in CVR findings between this study and others^{8,30,32} can be explained by differences in genetics of the mouse models, by differences in baseline perfusion states, or by differences in the study set-up, including the anaesthesia protocol. Although we did not find evidence for overt functional cerebrovascular deficits in our mouse model, this humanized mouse model captures early markers of CADASIL pathology, making it suitable for therapeutic studies targeting human mutant *NOTCH3*^{ECD} accumulation early in the disease course.

In summary, we show progression of GOM deposits in a humanized CADASIL mouse model. We propose a 5-stage GOM classification system for uniform assessment of GOM depositions in translational research. In future pre-clinical studies of therapeutic approaches aimed at reducing or preventing *NOTCH3*^{ECD} aggregation, GOM classification may serve as a valuable tool to monitor therapeutic efficiency on an ultrastructural level.

APPENDIX

Acknowledgements

We acknowledge the financial support from the Netherlands Brain Foundation (HA2016-02-03). We thank Baudouin Denis de Senneville for his help with the MR image registration; Lydiane Hirschler and Emmanuel Barbier for their help with the pCASL sequence; Sandra van Heiningen and the LUMC animal facility for mouse breeding; and Peter Neeskens for electron microscopy sample preparation.

Funding

This work was funded by the Netherlands Brain Foundation (HA2016-02-03).

Ethical approval

All applicable international, national, and/or institutional guidelines for the care and use of animals were followed. Experiments were approved by the local animal ethics committee (code 14073) and conducted in accordance with recommendations of the European Communities Council Directive (2010/63/EU) and ARRIVE guidelines. All efforts were made to minimize animal suffering. Except from using post-mortem material, this article does not contain any studies with human participants performed by any of the authors.

Disclosures

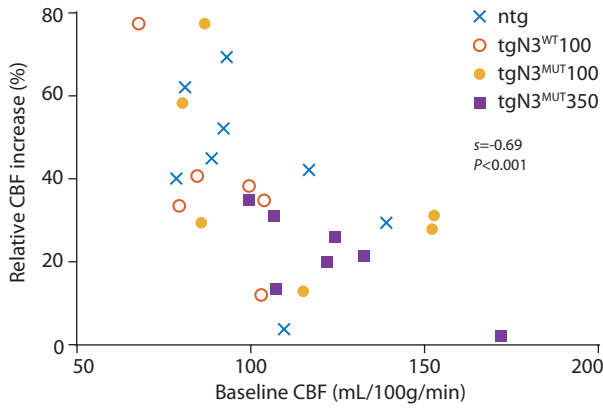
CG, JWR and SAJLO were supported by the Netherlands Brain Foundation (HA2016-02-03). SAJLO is co-inventor on an LUMC owned patent, not related to this work. LPM and LvdW were supported by NWO-VIDI (864.13.014). MO, AAM, IH, MD, AJK, SGvD, OCM, CRJ and AMJMVdM have nothing to disclose. AAR has nothing to disclose related to this work. For full transparency, she discloses being employed by LUMC and being co-inventor on several LUMC owned patents. As such she is entitled to a share of royalties. AAR further discloses being ad hoc consultant for PTC Therapeutics, BioMarin Pharmaceuticals Inc., Global Guidepoint, GLG consultancy, Grunenthal, Eisai, Sarepta Therapeutics and BioClinica, and having been a member of the Duchenne Network Steering Committee (BioMarin) and of the scientific advisory boards of ProQR and Philae Pharmaceuticals. Remuneration for these activities is paid to LUMC. LUMC also received speaker honoraria from PTC Therapeutics and BioMarin Pharmaceuticals.

REFERENCES

- Chabriat, H., Joutel, A., Dichgans, M., Tournier-Lasserre, E. & Bousser, M.-G. Cadasil. *Lancet. Neurol.* **8**, 643–53 (2009).
- Joutel, A. *et al.* Strong clustering and stereotyped nature of Notch3 mutations in CADASIL patients. *Lancet* **350**, 1511–5 (1997).
- Joutel, A. *et al.* Notch3 mutations in CADASIL, a hereditary adult-onset condition causing stroke and dementia. *Nature* **383**, 707–10 (1996).
- Ishiko, A. *et al.* Notch3 ectodomain is a major component of granular osmiophilic material (GOM) in CADASIL. *Acta Neuropathol.* **112**, 333–339 (2006).
- Monet-Leprêtre, M. *et al.* Abnormal recruitment of extracellular matrix proteins by excess Notch3 ECD: A new pathomechanism in CADASIL. *Brain* **136**, 1830–1845 (2013).
- Arboleda-Velasquez, J. F. *et al.* Hypomorphic Notch 3 alleles link Notch signaling to ischemic cerebral small-vessel disease. *Proc. Natl. Acad. Sci.* **108**, E128–E135 (2011).
- Yamamoto, Y. *et al.* Brain microvascular accumulation and distribution of the NOTCH3 ectodomain and granular osmiophilic material in CADASIL. *J. Neuropathol. Exp. Neurol.* **72**, 416–431 (2013).
- Ghosh, M. *et al.* Pericytes are involved in the

- pathogenesis of cerebral autosomal dominant arteriopathy with subcortical infarcts and leukoencephalopathy. *Ann. Neurol.* **78**, 887–900 (2015).
9. Gu, X., Liu, X.-Y., Fagan, A., Gonzalez-Toledo, M. E. & Zhao, L.-R. Ultrastructural Changes in Cerebral Capillary Pericytes in Aged Notch3 Mutant Transgenic Mice. *Ultrastruct. Pathol.* **36**, 48–55 (2012).
 10. Joutel, A. *et al.* The ectodomain of the Notch3 receptor accumulates within the cerebrovasculature of CADASIL patients. *J. Clin. Invest.* **105**, 597–605 (2000).
 11. Brulin, P., Godfraind, C., Leteurtre, E. & Ruchoux, M.-M. Morphometric analysis of ultrastructural vascular changes in CADASIL: analysis of 50 skin biopsy specimens and pathogenic implications. *Acta Neuropathol.* **104**, 241–8 (2002).
 12. Tikka, S. *et al.* Congruence between NOTCH3 mutations and GOM in 131 CADASIL patients. *Brain* **132**, 933–939 (2009).
 13. Morroni, M. *et al.* Role of Electron Microscopy in the Diagnosis of Cadasil Syndrome: A Study of 32 Patients. *PLoS One* **8**, 6–11 (2013).
 14. Ruchoux, M. M. *et al.* Systemic vascular smooth muscle cell impairment in cerebral autosomal dominant arteriopathy with subcortical infarcts and leukoencephalopathy. *Acta Neuropathol.* **89**, 500–512 (1995).
 15. Kalimo, H. *et al.* CADASIL: Hereditary disease of arteries causing brain infarcts and dementia. *Neuropathol. Appl. Neurobiol.* **25**, 257–265 (1999).
 16. Miao, Q. *et al.* Arterioles of the lenticular nucleus in CADASIL. *Stroke* **37**, 2242–2247 (2006).
 17. Gatti, J. R. *et al.* Redistribution of Mature Smooth Muscle Markers in Brain Arteries in Cerebral Autosomal Dominant Arteriopathy with Subcortical Infarcts and Leukoencephalopathy. *Transl. Stroke Res.* **10**, 160–169 (2019).
 18. Yamamoto, Y. *et al.* Neuropathological correlates of temporal pole white matter hyperintensities in CADASIL. *Stroke* **40**, 2004–2011 (2009).
 19. Dong, H. *et al.* Advanced intimal hyperplasia without luminal narrowing of leptomeningeal arteries in CADASIL. *Stroke* **44**, 1456–1458 (2013).
 20. Pfefferkorn, T. *et al.* Reduced cerebrovascular CO(2) reactivity in CADASIL: A transcranial Doppler sonography study. *Stroke* **32**, 17–21 (2001).
 21. Chabriat, H. *et al.* Cerebral hemodynamics in CADASIL before and after acetazolamide challenge assessed with MRI bolus tracking. *Stroke* **31**, 1904–12 (2000).
 22. Rutten, J. W. *et al.* The NOTCH3 score: a pre-clinical CADASIL biomarker in a novel human genomic NOTCH3 transgenic mouse model with early progressive vascular NOTCH3 accumulation. *Acta Neuropathol. Commun.* **3**, 89 (2015).
 23. Faas, F. G. A. *et al.* Virtual nanoscopy: Generation of ultra-large high resolution electron microscopy maps. *J. Cell Biol.* **198**, 457–469 (2012).
 24. Dodds, H. M. & Clark, G. An improved Van Gieson. *Stain Technol.* **60**, 55 (1985).
 25. Lewandowska, E., Dziewulska, D., Parys, M. & Pasennik, E. Ultrastructure of granular osmiophilic material deposits (GOM) in arterioles of CADASIL patients. *Folia Neuropathol.* **49**, 174–80 (2011).
 26. Lewandowska, E., Felczak, P., Buczek, J., Gramza, K. & Rafałowska, J. Blood vessel ultrastructural picture in a CADASIL patient diagnosed at an advanced age. *Folia Neuropathol.* **4**, 443–451 (2014).
 27. Ruchoux, M. M. *et al.* Transgenic Mice Expressing Mutant Notch3 Develop Vascular Alterations Characteristic of Cerebral Autosomal Dominant Arteriopathy with Subcortical Infarcts and Leukoencephalopathy. *Am. J. Pathol.* **162**, 329–342 (2003).
 28. Monet, M. *et al.* The archetypal R90C CADASIL-NOTCH3 mutation retains NOTCH3 function in vivo. *Hum. Mol. Genet.* **16**, 982–992 (2007).
 29. Monet-Lepretre, M. *et al.* Distinct phenotypic and functional features of CADASIL mutations in the Notch3 ligand binding domain. *Brain* **132**, 1601–1612 (2009).
 30. Joutel, A. *et al.* Cerebrovascular dysfunction and microcirculation rarefaction precede white matter lesions in a mouse genetic model of cerebral ischemic small vessel disease. *J. Clin. Invest.* **120**, 433–445 (2010).
 31. Miao, Q. *et al.* Fibrosis and Stenosis of the Long Penetrating Cerebral Arteries: the Cause of the White Matter Pathology in Cerebral Autosomal Dominant Arteriopathy with Subcortical Infarcts and Leukoencephalopathy. *Brain Pathol.* **14**, 358–364 (2006).
 32. Lacombe, P., Oligo, C., Domenga, V., Tournier-Lasserre, E. & Joutel, A. Impaired Cerebral Vasoreactivity in a Transgenic Mouse Model of Cerebral Autosomal Dominant Arteriopathy With Subcortical Infarcts and Leukoencephalopathy Arteriopathy. *Stroke* **36**, 1053–1058 (2005).

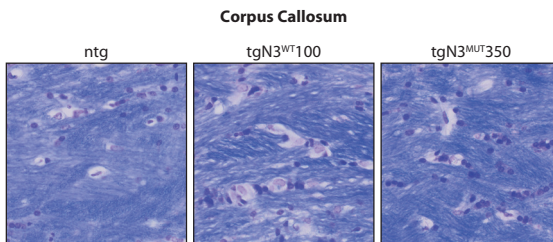
SUPPLEMENTARY DATA



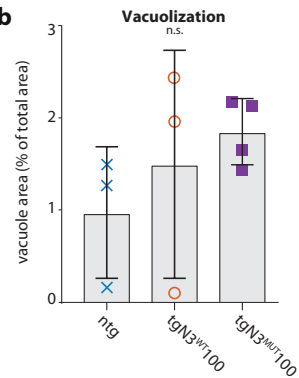
Supplementary Data 2.1: Baseline CBF correlates with CVR in CADASIL mice

Relative CBF increase (CVR) was determined for all mouse strains (ntg, tgN3^{WT}100, tgN3^{MUT}100, tgN3^{MUT}350). CVR values were negatively associated with baseline CBF values ($s = -0.69$, $P < 0.001$), suggesting that CVR represents differences in both baseline CBF and actual vascular reactivity.

a

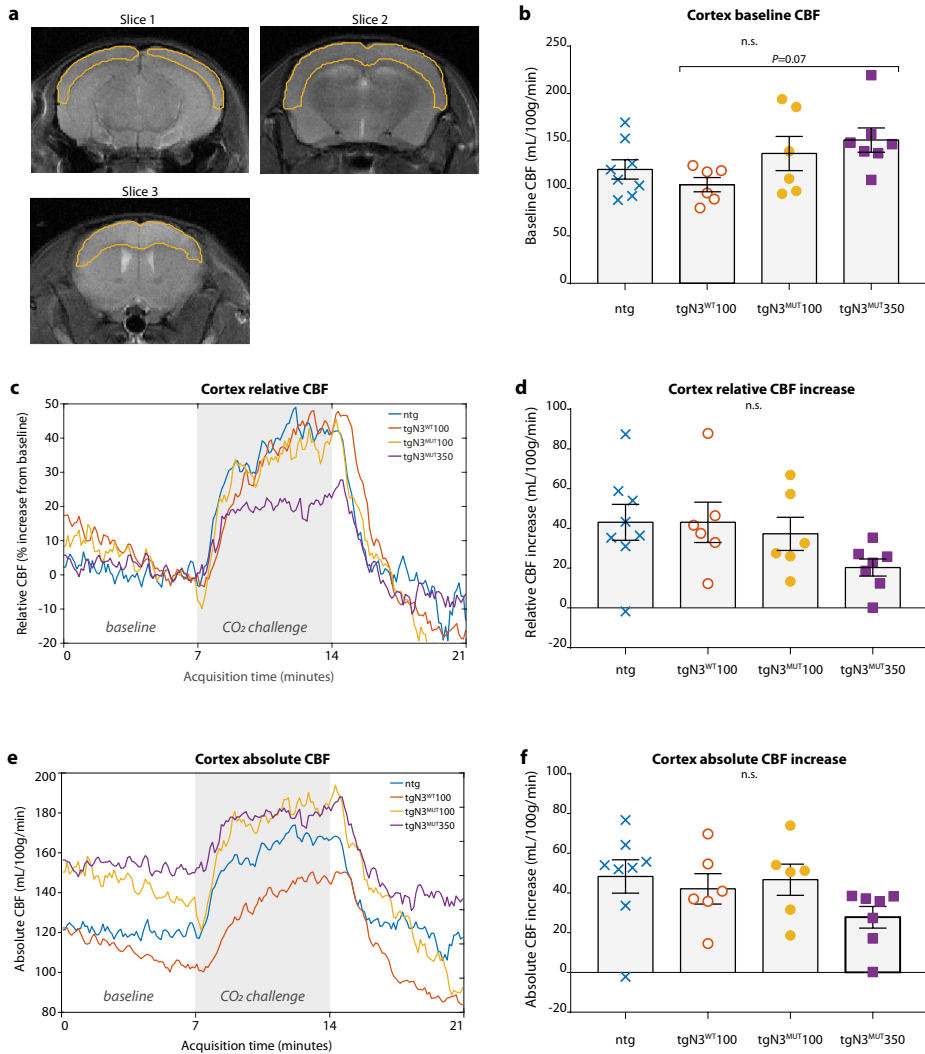


b



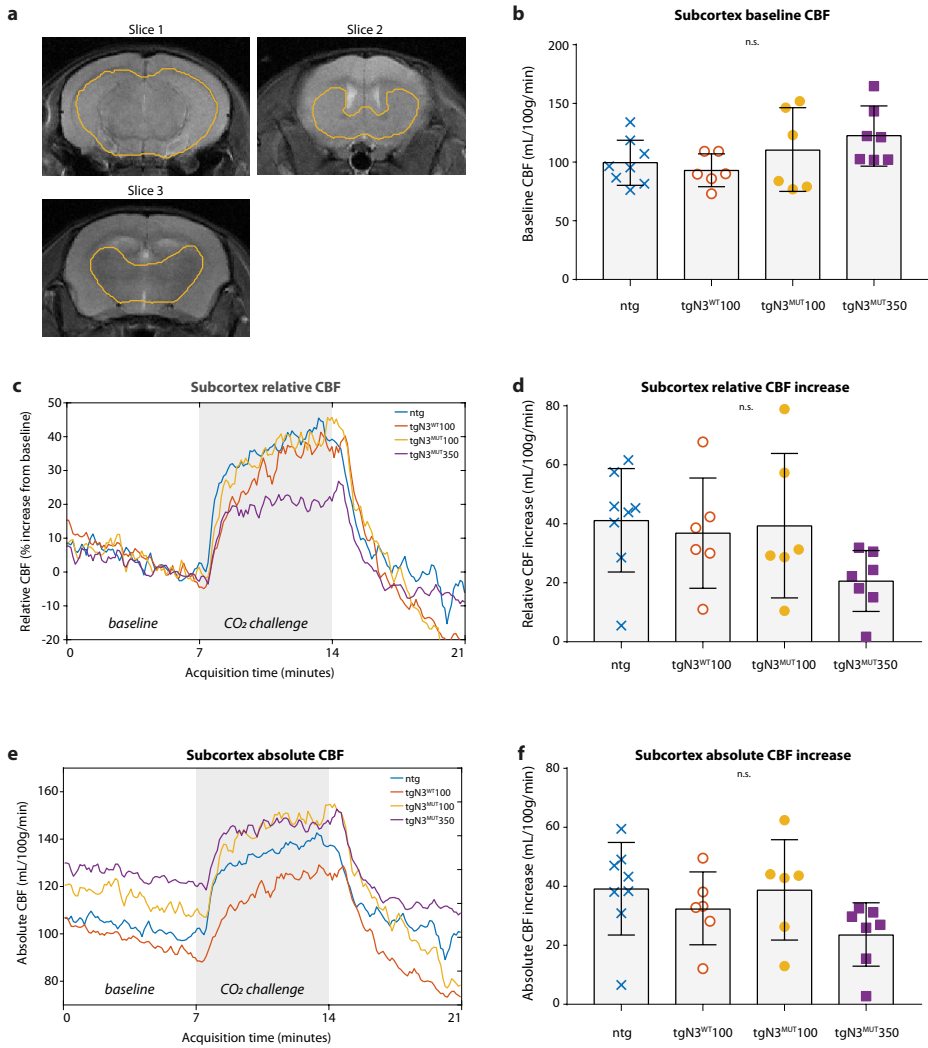
Supplementary Data 2.2: CADASIL mice do not show increased levels of vacuolization

(A) Representative images of Klüver-Barrera luxol fast blue staining of the corpus callosum in 20-month-old non-transgenic mice (ntg), wildtype mice (tgN3^{WT}100) and mutant mice (tgN3^{MUT}350). (B) Quantification of the vacuole area in the corpus callosum, showing similar levels of vacuolization (ntg 0.98%±0.71%, tgN3^{WT}100 1.51%±0.71%, tgN3^{MUT}350 1.86%±0.36%, $P = 0.40$, ANOVA). Graph represent mean±SD; n.s. = non significant.



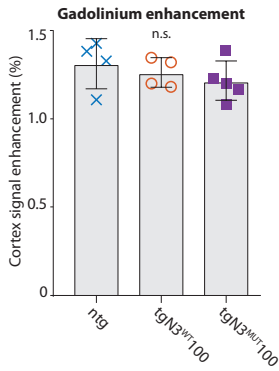
Supplementary Data 2.3: CADASIL mice do not show altered cortical cerebrovascular reactivity

(A) Region-of-interest of cortex. (B) Baseline CBF in cortex was similar among the groups (ntg, tgN3^{WT}100, tgN3^{MUT}100, tgN3^{MUT}350). (C,D) Average relative CBF profiles over time are shown for cortex. CVR was similar in all groups. (E,F) Average absolute CBF profiles over time. Absolute CBF rise upon CO₂ challenge was similar between the groups. Graphs represent mean or mean±SD; n.s. = non significant.



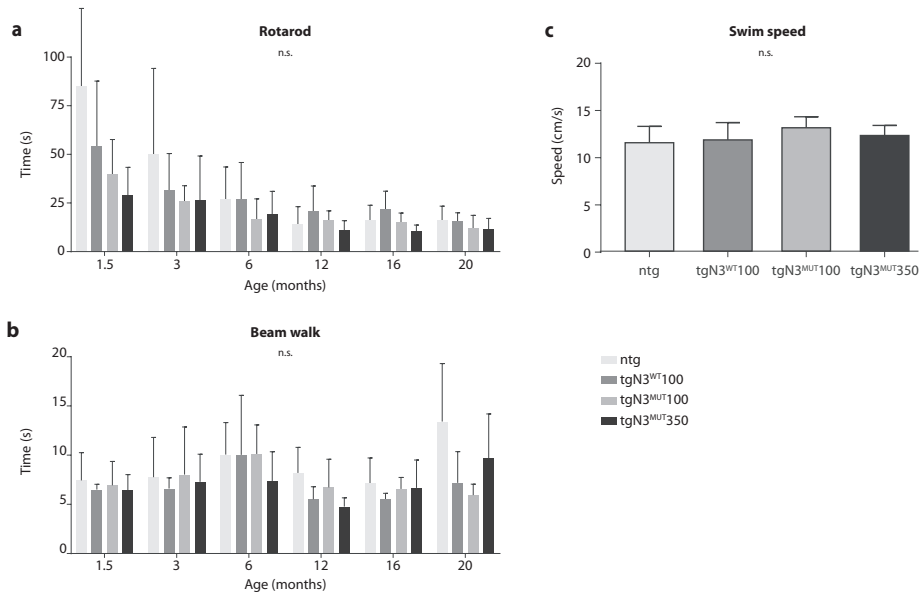
Supplementary Data 2.4: CADASIL mice do not show altered subcortical cerebrovascular reactivity

(A) Region-of-interest of subcortex. (B) Baseline CBF in subcortex was similar among the groups (ntg, tgN₃^{WT}100, tgN₃^{MUT}100, tgN₃^{MUT}350). (C,D) Average relative CBF profiles over time are shown for subcortex. CVR was similar in all groups. (E,F) Average absolute CBF profiles over time. Absolute CBF rise upon CO₂ challenge was similar between the groups. Graphs represent mean or mean \pm SD; n.s. = non significant.



Supplementary Data 2.5: CADASIL mice do not show blood brain barrier leakage

Blood brain barrier function was assessed in a second cohort of ntg (n=4), tgN3^{WT100} (n=4), and tgN3^{MUT350} (n=5) mice at the age of 12 months by determining Gadolinium-induced signal enhancement on brain MRI after injection of Gadolinium. No differences in signal enhancement were observed (ntg 1.31%±0.14%, tgN3^{WT100} 1.26%±0.08%, tgN3^{MUT350} 1.22%±0.11%, P=0.48, ANOVA).



Supplementary Data 2.6: CADASIL mice do not show motor dysfunction

Bar charts showing (A) the time to complete a beam walk and (B) the time without falling of a rotarod for all groups (ntg, tgN3^{WT100}, tgN3^{MUT100}, tgN3^{MUT350}) at various time points. No differences were seen between groups on the beam walk and rotarod motor function tests. (C) Average swimming speed from all trainings and reversal trainings was similar between groups. Graphs represent mean±SD; n.s. = non significant.

Supplementary Data 2.7: Physiology parameters during cerebral hemodynamic assessment at baseline and at CO₂ challenge in CADASIL mice

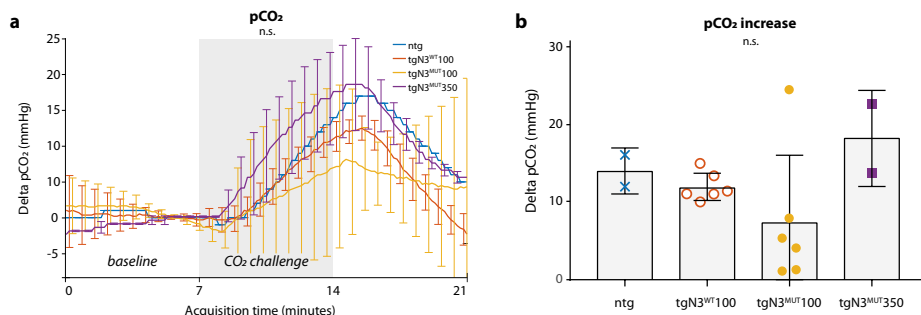
	Baseline mean (sd) <i>P-value</i> ^a	CO ₂ challenge mean (sd) <i>P-value</i> ^a	<i>P-value</i> ^b
Body temperature (°C)	n.s.	n.s.	
ntg	35.4 (2.0)	35.3 (2.4)	n.s.
tgN3 ^{WT} 100	35.3 (0.4)	35.6 (0.5)	n.s.
tgN3 ^{MUT} 100	34.4 (0.5)	34.5 (0.9)	n.s.
tgN3 ^{MUT} 350	35.2 (1.3)	35.5 (1.2)	<i>P</i> =0.006
Respiration (/min)	n.s.	n.s.	
ntg	154 (34)	157 (33)	n.s.
tgN3 ^{WT} 100	125 (32)	127 (45)	n.s.
tgN3 ^{MUT} 100	112 (45)	131 (37)	n.s.
tgN3 ^{MUT} 350	160 (28)	191 (50)	<i>P</i> =0.031
Oxygenation (%)	n.s.	n.s.	
ntg	78 (17)	77 (16)	n.s.
tgN3 ^{WT} 100	72 (15)	72 (18)	n.s.
tgN3 ^{MUT} 100	74 (15)	85 (4)	n.s.
tgN3 ^{MUT} 350	86 (11)	90 (7)	n.s.
Heart rate (/min)	n.s.	<i>P</i> =0.009 ^c	
ntg	306 (73)	315 (82) ^c	n.s.
tgN3 ^{WT} 100	225 (20)	209 (22) ^c	n.s.
tgN3 ^{MUT} 100	300 (115)	269 (23)	n.s.
tgN3 ^{MUT} 350	285 (51)	290 (30)	n.s.

^a *P*-value per tested physiology parameter represent ANOVA *P*-value for testing differences between groups at baseline and differences between groups at challenge.

^b *P*-value represent paired student's *t*-test between baseline and challenge values of the parameter within the respective mouse strain.

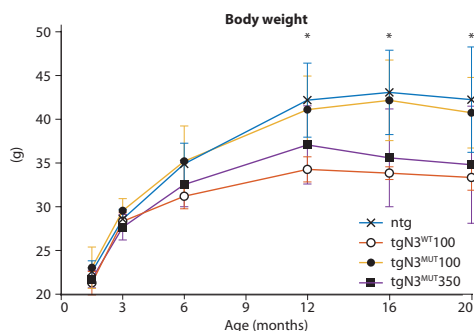
^c Heart rate during CO₂ challenge was significantly different between the different mouse strains. Post-hoc testing showed that tgN3^{WT}100 mice had significantly lower heart rates than ntg (*P*=0.006).

n.s. = non significant.



Supplementary Data 2.8: pCO₂ in blood increase upon CO₂ challenge

(A) Absolute pCO₂ increase is plotted over time. pCO₂ levels were normalized to zero at baseline. (B) No significant differences in pCO₂ increase between the mouse strains (ntg, tgN₃^{WT100}, tgN₃^{MUT100}, tgN₃^{MUT350}). Please note that pCO₂ measurements of only a subset of mice is plotted (ntg n=1; tgN₃^{WT100} n=6; tgN₃^{MUT100} n=6; tgN₃^{MUT350} n=2) as the pCO₂ datasets of the other mice were lost due to technical reasons. Graphs represent mean±SD; n.s. = non significant.



Supplementary Data 2.9: Reduced body weight in tgN₃^{MUT350} and tgN₃^{WT100} mice compared to ntg and tgN₃^{MUT100} mice

Mice showed similar weights at younger ages, but from the age of 12 months, tgN₃^{WT100} mice were significantly lighter than ntg mice, and from the age of 16 months, tgN₃^{WT100} and tgN₃^{MUT350} mice were significantly lighter than tgN₃^{MUT100} and ntg mice (ntg 43.1±4.8 g, tgN₃^{WT100} 33.8±0.7 g, tgN₃^{MUT100} 42.2±4.6 g, tgN₃^{MUT350} 35.6±5.6 g, P=0.003; ANOVA). *P<0.05. Graph represents mean±SD.

SUPPLEMENTARY METHODS

Supplementary Methods 1: Neuroimaging and CVR assessment

Anaesthesia and physiological monitoring during neuroimaging

Mice were anesthetized with 3.5% isoflurane in medical air enriched with oxygen (75% air, 25% oxygen) for 4 minutes, followed by a continuous flow of 2% isoflurane during positioning of the mouse in the animal bed of the MRI scanner. A subcutaneous catheter was placed to infuse medetomidine (Dexdomitor, Vetoquinol SA, Lure, France [a solution without the inactive enantiomer levomedetomidine]) with a syringe pump (Univentor 802, Univentor High Precision Instruments, Zejtun, Malta). At the beginning of image acquisition, a bolus of 0.15 mg/kg medetomidine was injected, and 10 minutes later followed by a continuous infusion of 0.30 mg/kg/hr medetomidine. During those 10 minutes, the isoflurane concentration was slowly reduced to 0%, while the administration of the air/oxygen mixture was continued. During image acquisition, respiration was registered using a pressure pad placed underneath the animal. Heart rate and pulse oxygenation (both SA instruments, New York, USA) were recorded using an infrared probe around the leg. Changes in transcutaneous (tc)-pCO₂ values were measured using a tc-pCO₂ sensor (TCM radiometer, Zoetermeer, The Netherlands) placed on shaved skin on the flank of the animal. Temperature was maintained using a feedback-controlled waterbed (Medres, Cologne, Germany). Directly after neuroimaging, still under anaesthesia, mice were decapitated and tissue was collected.

MR image acquisition for cerebral hemodynamic assessment

MR images were acquired with a 7 T Bruker PharmaScan (Ettlingen, Germany) using a 23 mm volume coil. Anatomical T2 Turbo RARE scans were acquired in all three directions for planning of the arterial spin labelling (ASL) scans with the following parameters: TE/TR = 35.0 ms/2,500 ms, 0.7 mm slice thickness without a slice gap, 1 average, matrix of 256 by 256, field of view of 21.55 by 21.55 mm, RARE factor of 8, and a bandwidth of 36.7 kHz. To aid image registration, three slices of 1.5 mm thick with the same imaging parameters as above and the same geometry as the pseudo-continuous arterial spin labeling (pCASL) scans were acquired. The pCASL sequence was used to image the cerebral blood flow (CBF) and cerebrovascular reactivity (CVR, i.e. relative CBF increase). The label and control interpulse-phases of the sequence were optimized beforehand, to correct for off-resonance effects [1]. The labelling plane was placed in the neck, 1.0 cm from isocenter. Three 1.5 mm thick single-shot, spin-echo - Echo Planar Imaging (EPI) slices were used with a slice gap of 1 mm, where the middle slice was placed at isocenter and at -0.75 mm Bregma. The following imaging parameters were used: TE/TR = 16.8 ms/3,520 ms, labelling duration (τ) of 3,000 ms, post-label delay (PLD) of 300 ms, FOV of 21.55 x 21.55 mm and a matrix of 96 x 96. 180 pairs of label/control images (repetitions) were acquired, with a total pCASL imaging duration of 21 minutes. During the challenge, i.e. between minute 7 and 14 and

between repetition 60 to repetition 120, 7.5% CO₂ was added to the gas mixture. T1 maps were acquired using an inversion recovery EPI with 18 inversion times and with the same geometry as the pCASL sequence. Labelling efficiency (α) was measured 0.3 cm downstream the labelling plane with a flow-compensated, ASL-encoded FLASH sequence. The latter two sequences were used to support CBF-quantification. After the pCASL scan, three additional anatomical scans were acquired with the following details: (1) a high resolution T2W sequence with TE/TR = 39 ms/2,200 ms, a matrix of 384 x 384, 9 slices with a thickness of 0.7 mm, a 0.3 mm slice gap and 8 averages; (2) a T2W-Fluid-Attenuated Inversion Recovery (FLAIR) sequence with TE/TR = 37 ms/1,000 ms, a matrix of 192 x 192, 9 slices with a thickness of 1.0 mm, without a slice gap and 3 averages; and (3) a Susceptibility-Weighted Imaging (SWI) sequence with TE/TR = 18 ms/350 ms, a matrix of 384 x 384, 9 slices with a thickness of 0.7 mm, a 0.3 mm slice gap and 5 averages. These three sequences were acquired in the same orientation and with the same FOV as the pCASL scan.

MR image registration and processing

Individual pCASL EPIs and individual inversion recovery EPIs were aligned to the first label magnitude image of the pCASL sequence using a MATLAB monomodal rigid body registration with 300 iterations (MATLAB version R2016a, Mathworks, Natick, USA). The anatomical T2RARE images of one dataset were used to delineate the cortex and the full brain. These regions of interest (ROIs) were automatically propagated to the T2RARE images of the other datasets, and subsequently to the EPIs of every dataset. An edge-based variational method for non-rigid multimodal registration was used to propagate the ROIs [2]. The results of both propagation steps were verified for each dataset by an operator (L.P.M.).

Buxton's general kinetic perfusion model was used to quantify cerebral blood flow (CBF) from the measured difference between label and control acquisition (Buxton et al., *Magn Reson Med.* 1998;40:383-396), *i.e.* the following equation was used:

$$\text{CBF} = [\lambda \cdot \Delta M \cdot \exp(\text{PLD} / T_{1b})] / [2 \cdot \alpha \cdot T_{1T} \cdot (1 - \exp(-\tau / T_{1T}))]$$

Here, ΔM is the measured difference between the label and control EPIs, T_{1b} is the T1 of blood at 7 T, assumed to be 2230 ms [3]. Also, it is assumed that at thermal equilibrium, the magnetization of arterial blood (M_{ob}) may be approximated by M_{ot}/λ , where M_{ot} is the magnetization of tissue and λ is 0.9, the blood–brain partition coefficient of water [4]. Baseline CBF was defined as the mean CBF of the 20 repetitions before the onset of the CO₂ challenge, which is equal to 2 minute 20 seconds before the onset. CBF during CO₂ was defined as the mean of the 20 repetitions before the end of the CO₂. These two estimates were used to calculate cerebrovascular reactivity (CVR) by using the following equation: $\text{CVR} (\%) = [\text{mean CBF during challenge} - \text{mean CBF during baseline}] / [\text{mean CBF during baseline}] \cdot 100\%$

MR image acquisition for blood brain barrier assessment using Gadolinium

Blood brain barrier function was assessed in a second cohort of ntg (n=4), tgN3WT100 (n=4), and tgN3MUT350 (n=5) mice at the age of 12 months by determining Gadolinium-induced signal enhancement on brain MRI after injection of Gadolinium. Gadolinium-DOTA (Dotarem, Guerbet, Cedex, France) was administered intra-peritoneally at 10 mmol/kg. MRI was performed using a series of consecutive T1W images with a RARE sequence (TR/TE = 870/11.7 ms, matrix size = 256 x 256, field-of-view = 20 x 20 mm², number of averages = 6, slice thickness = 0.5 mm, coronal slices, RARE factor = 2), both before (1 image) and after (6 images) contrast agent administration. The 6 post-contrast images have been acquired immediately after the contrast agent injection, thus started at 0 min, 12 min, 24 min, 36 min, 48 min, and 60 min post-injection, respectively. Blood brain barrier leakage was calculated as percentage signal enhancement after contrast in a region-of-interest placed on the cortex at Bregma -2 mm. Signal enhancement was calculated as the relative change in signal intensity (SI) between pre- and the last post-contrast T1W image (ΔSI) as per the following equation, $\Delta SI = [SI(t) - SI(0)] / SI(0)$, where SI(t) is the signal intensity at time t after Gadolinium-DOTA injection and SI(0) is the signal intensity of the selected region-of-interest in the scan prior to Gadolinium-DOTA injection.

Supplementary Methods 2: Cognitive assessment

A Morris water maze protocol was used to assess cognitive function, as it is considered to be a valid measure of hippocampal dependent spatial navigation and reference memory. The swimming pool (diameter 138cm) was filled with opaque white water (by adding non-toxic paint) which was maintained at a temperature of 20-22°C. A platform (diameter 10.8 cm, platform pool ratio 1:163) was placed 5-8 mm under the water surface in the north-west quadrant and south-east quadrant during the training phase and reversal training phase, respectively. Ten cm from the pool, three high contrast figures were placed to facilitate spatial navigation. To prevent praxic and taxic navigation rather than spatial navigation, mice were released from different locations during the experiment.

Three days before starting the training phase, mice were allowed to swim in the pool for 2 min. Mice underwent 4 trials for 5 or 4 days during the training phase or reversal training phase, respectively, where they had a maximum of 120 seconds per trial to locate the hidden platform. After the trial, regardless whether they found the platform, mice were placed on the platform for 15 seconds allowing them to remember the location. Three days after the training phase and reversal training phase, mice were placed for 2 minutes in the swimming pool of which the platform was removed (no platform test and reversal no platform test, respectively). Mice were recorded using the Noldus EthoVision® XT Base software (version 11.5). Path length to platform was used as outcome measure for (reversal) training phase and time per quadrant for the no-platform tests.

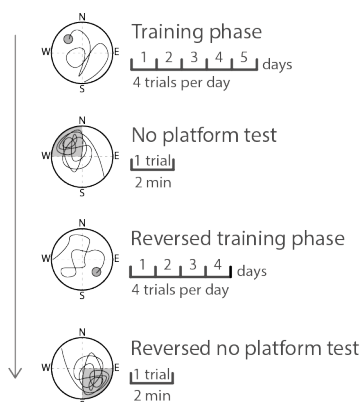


Figure: Graphical summary experimental design Morris water maze protocol

Supplementary Methods 3: Motor function tests

For rotarod tests, mice had to run on a rotating rod (speed gradually increasing up to 45 rpm) for a maximum of 5 minutes. For beam walk tests, time to cross a beam of 80 cm with a diameter of 11 mm was recorded. As we noted that all mice had difficulty performing the task, from the age of 6 months, the diameter of the beam was increased to 17 mm. Mice took three trials per time point and the average time was analysed for both tests. Average swimming speed was calculated based on all MWM trials.

Supplementary Methods 4: Quantification of vacuolization in mouse brain

Two 5- μ m brain sections per mouse were analysed after staining them with Klüver-Barrera luxol fast blue staining according to standard protocol. Corpus callosum was captured at 400x with the same capture settings for all sections. Regions-of-interest were manually drawn around the corpus callosum, thereby excluding blood vessel area if vessels were present in the image. Vacuoles were quantified using ImageJ thresholding for the vacuole areas. Vacuole area is expressed as vacuole area percentage compared to total region-of-interest area. Multiple measurements were averaged per mouse.

Supplementary References

- Hirschler L, Debacker CS, Voiron J, Köhler S, Warnking JM, Barbier EL. Interpulse phase corrections for unbalanced pseudo-continuous arterial spin labeling at high magnetic field. *Magn Reson Med.* 2018;79:1314–24.
- Denis De Senneville B, Zachiu C, Ries M, Moonen C. Evolution: An edge-based variational method for non-rigid multi-modal image registration. *Phys Med Biol.* IOP Publishing; 2016;61:7377–96.
- Dobre MC, Uğurbil K, Marjanska M. Determination of blood longitudinal relaxation time (T_1) at high magnetic field strengths. *Magn Reson Imaging.* 2007;25:733–5.
- Herscovitch P, Raichle ME. What is the correct value for the brain–blood partition coefficient for water? *J Cereb Blood Flow Metab.* 1985;5:65–9.

